



STAR FORMATION

Survey of H α emission-line stars in the star-forming region IC 5070

NEELAM PANWAR^{1,*} , JESSY JOSE² and C. RISHI¹

¹Aryabhata Research Institute of Observational Sciences, Nainital 263001, India.

²Indian Institute of Science Education and Research (IISER) Tirupati, Rami Reddy Nagar, Karakambadi Road, Mangalam (P.O.), Tirupati 517507, India.

*Corresponding author. E-mail: neelam@aries.res.in

MS received 16 November 2022; accepted 25 January 2023

Abstract. Actively accreting young stellar objects show H α emission line in their spectra. We present the results of survey for H α emission-line stars in the star-forming region IC 5070 taken with 2-m Himalyan Chandra Telescope. Based on the H α slitless spectroscopy data, we identified 131 emission-line stars in ~ 0.29 square degrees area of the IC 5070 region. Using Gaia early data release 3, we estimated the mean proper motion and parallax of the emission-line stars. We also estimated the mean distance and reddening toward the region using the emission-line stars, which are ~ 833 pc and ~ 2 mag, respectively. By examining the locations of these stars in the color–magnitude diagrams constructed using Gaia and PanSTARRS1 data, we found that a majority of the H α emitters are young low-mass ($< 1.5 M_{\odot}$) stars. We also compared our catalog of emission-line stars with the available young stellar catalogs and found that most of them are class II/flat spectrum sources with the spectral type ranging from K to M. Based on the proper motion/parallax values and locations on the color–magnitude diagrams, about 20 emission-line stars are flagged as non-members. The relative proper motion of the emission-line stars with respect to the ionizing source suggest the possibility of the ‘rocket effect’ scenario in the remnant cloud (BRC 31).

Keywords. HII regions: IC 5070—stars: T-Tauri—stars: proper-motion.

1. Introduction

Stars form from dense molecular clouds in star-forming regions (SFRs) and a majority of these emerge as groups/clusters. The spatial distribution of young stars and gas in SFRs can predict the initial conditions in which these stars are formed (e.g., [Gouliermis 2018](#); [Kuhn et al. 2020](#)). In addition to the above, for nearby SFRs, a sample of young stars obtained with the photometric observations can provide a complete knowledge of clustered or scattered populations ([Getman et al. 2018](#); [Herczeg et al. 2019](#); [Panwar et al. 2019](#); [Gupta et al. 2021](#)). H α emission is one of the signatures used to identify young T-Tauri stars (TTSs), which arises due to the ongoing accretion process associated with these stars. Though, objective prism surveys for H α emission stars were the first technique to identify large populations of young stars (e.g., [Haro 1953](#); [Herbig 1954](#)),

with the advent of CCDs combined with grisms, much deeper surveys were possible (e.g., [Herbig 1998](#); [Herbig & Dahm 2006](#); [Pettersson & Reipurth 2019](#)). We performed a slitless H α survey for the search of the H α emission stars in the star-forming region IC 5070.

The star-forming region IC 5070 (also known as the Pelican nebula) in Cygnus has received special attention and has become the target of many observational studies for last two decades. It is associated with the HII region Sh2-117 or W80 ([Westerhout 1958](#)). The nebula is adjacent to the North-American Nebula (NGC 7000), which is now considered as a part of the same physical gas and dust cloud ([Reipurth & Schneider 2008](#)). The whole NGC 7000/IC 5070 cloud complex, also known as the North American and Pelican (NAP) complex, encloses many active star-forming sites with strong obscuration attributed to the high amount of gas and dust. The main exciting source of the HII region is 2MASS J20555125+4352246 (O3.5f*+O8) spectroscopic binary ([Comerón & Pasquali 2005](#); [Maíz Apellániz et al. 2016](#)), lying between the NGC 7000 and

This article is part of the Special Issue on “Star formation studies in the context of NIR instruments on 3.6m DOT”.

IC 5070 and is embedded within the highly extinguished ($A_V \sim 9.6$ mag) dark dust cloud LDN 935. Though there is one more massive star, HD 199579 (O6.5 V; Sota *et al.* 2011), it is at larger distance and quite away from the geometrical center of the HII region, therefore, unlikely to be a main ionizing source.

A number of H α emission-line stars and many Herbig-Haro objects have been found in the region (Herbig 1958; Ogura *et al.* 2002; Bally & Reipurth 2003; Bally *et al.* 2014). High sensitivity infrared (IR) and X-ray observations with the Spitzer and Chandra X-ray observatories (Guieu *et al.* 2009; Rebull *et al.* 2011; Damiani *et al.* 2017; Das *et al.* 2021) reveal several groups/clusters of young stars embedded in the whole NAP star-forming region. Presence of several protostars, cometary nebulae, bright-rimmed cloud (BRC) 31 and outflows driven by embedded young stars indicates ongoing active star formation throughout the region (Ogura *et al.* 2002; Bally & Reipurth 2003; Bally *et al.* 2014). Various studies yield different distance estimates for the NAP complex, ranging from about 500 pc to above 1 kpc (Laugalys *et al.* 2007; Reipurth & Schneider 2008; Guieu *et al.* 2009), with recent estimate based on the Gaia DR2 data placing it at ~ 800 pc (Bhardwaj *et al.* 2019; Zucker *et al.* 2020). Though located adjacent to the massive star-forming regions of Cygnus X, NAP is reported to be nearer than Cygnus X (Kuhn *et al.* 2020). Recent studies on the clustering and kinematic analyses of the NAP complex show that it contains several groups of very young stars associated with the observed molecular gas, which are at different distances, spanning differences up to 150–200 pc (Fang *et al.* 2020; Kuhn *et al.* 2020; Das *et al.* 2021).

The Pelican Nebula is among one of the ideal site to study the influence of massive stars on subsequent star-formation activity and evolution of the parental molecular clouds. However, the optical photometric studies of PMS stars in the region are available only for a limited sample (Findeisen *et al.* 2013; Poljančić *et al.* 2014; Ibryamov *et al.* 2018; Bhardwaj *et al.* 2019 and references therein). The BVRI photometry for a sample of 17 pre-main sequence (PMS) objects was presented by Poljančić *et al.* (2014) in the field of the NAP complex, while Froebrich *et al.* (2018) found two new low-mass young stars with deep recurring eclipses in the IC 5070.

The strong radiation field and the expanding HII region have cleared away some of the cloud surrounding the IC 5070 region, making part of the young stellar content visible at optical wavelengths. Such visible young stars are distinguishable based on H α emission line in

their spectra, which is caused by ongoing accretion processes from a circumstellar disk through funnel flows onto the star (Hartmann *et al.* 2016). Since the accretion of matter on the stellar surface is episodic, the H α emission is thus not stationary and is therefore, expected to be variable, although the timescale of variability is poorly known (Bhardwaj *et al.* 2019; Das *et al.* 2021; Ghosh *et al.* 2022). An advantage of using H α emission to identify young stars is that even stars with little circumstellar material, which are otherwise difficult to be identified as young through infrared photometric observations, can exhibit H α emission. H α emission-line surveys and IR surveys therefore, to some extent complement each other.

Slitless spectroscopy is a very efficient method to identify H α emission line sources compared to slit spectroscopy or IFU surveys, which are time consuming and expensive for telescopes. In the present work, we carried out slitless H α spectroscopic survey of ~ 0.29 square degrees region in the IC 5070 region to search for the H α emission-line stars. The organization of the paper is as follows. Section 2 present the observations, data reductions and the ancillary data obtained from published young star catalogs, Gaia early data release 3 (EDR3) and slitless spectroscopy used in this study. In Section 3, we describe the methods used to identify stellar members and characterization of the emission-line stars using photometric and kinematic information based on the Gaia EDR3 and PanSTARRS1 (PS1) data. Finally, Section 4 summarizes the main results of the present work.

2. Observations and data reduction

2.1 Optical slitless spectroscopy

We obtained slitless observations in H α for the IC 5070 region (see Figure 1, left panel) to detect H α emission line stars toward the region using the 2.0-m Himalayan Chandra Telescope (HCT) at Hanle. The observations were taken during the period of December–January 2012/2013. The details about the telescope and CCD camera can be found in Chauhan *et al.* (2009) and Jose *et al.* (2013). The data were acquired using a broadband H α filter (630–674 nm) in combination with Grism 5 (520–1030 nm) in slitless mode with the 2K \times 2K CCD. The CCD has a field-of-view (FOV) of 10 \times 10 arcmin². The data were taken for about 11 overlapping regions, covering a total sky area (~ 0.29 square degrees), shown in Figure 1. Images with a total integration of 1200 s

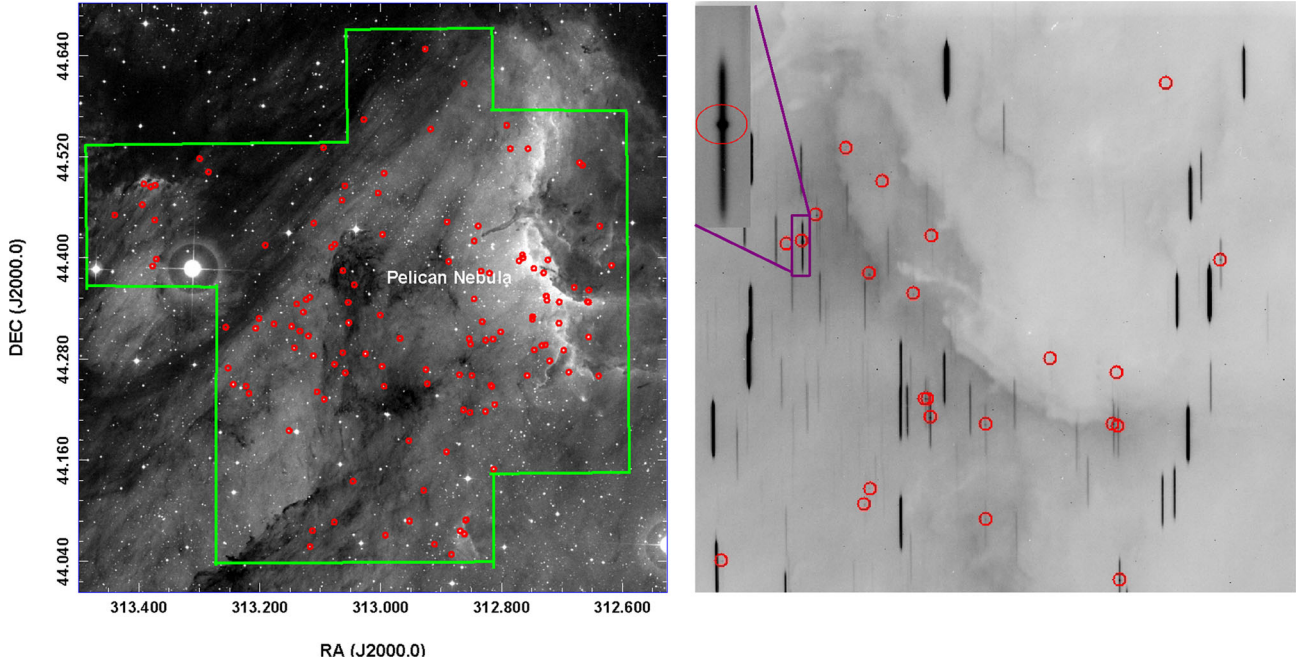


Figure 1. Left panel: DSS2R image of the IC 5070 region. Area enclosed with the green polygon represents the coverage of the present survey of H α emission-line stars with the HCT (~ 0.29 square degrees). The red circles represent emission-line stars identified in the present work. Right panel: Color-inverted slitless H α image for one of the sub-regions. Stars with enhanced H α emission are marked with the red circle.

in slitless mode, were taken for each region followed by an image in H α filter. The image in H α was used to identify the coordinates of the emission-line sources. To clean the images, a number of bias and twilight flat-field frames were taken. We have used IRAF software for the pre-processing of the raw images. The H α emitting sources show sharp enhancements in their spectra around 6563 Å over the continuum. Based on this signature, we identified 131 sources having prominent H α emissions from these observations, as shown in Figure 1 (right panel).

2.2 Ancillary data

2.2.1 Gaia EDR3 A sample of young stars obtained with the photometric observations complemented with astrometric information available with the Gaia data can be used to select the young members associated with the region. The Gaia mission has provided rich astrometric and photometric data for the stars. In the present work, we used Gaia EDR3 (Gaia Collaboration 2020) catalog to elucidate the kinematics and parallax of the emission-line stars in the region.

2.2.2 PanSTARRS data The Panoramic Survey Telescope and Rapid Response System (PanSTARRS) has carried out a 3π survey towards the northern sky

($\delta > -30^\circ$). The PS1 survey was carried out mainly at Haleakala Observatory in Hawaii in five broadband filters (g, r, i, z, y) from 2010 to 2014 (see, Chambers *et al.* 2016).

2.2.3 Available young star catalogs The whole NAP complex is one of the most active star-forming sites and has been a target to study the clustering of young stellar objects and molecular gas. Recently, low-resolution spectroscopic survey of over about 3400 young stars in the whole NAP complex by Fang *et al.* (2020) revealed about 580 likely members. Das *et al.* (2021) identified and characterized several young stars in the NAP complex using Spitzer and UKIDSS near-infrared (NIR) datasets. We have also utilized their young stellar catalogs (Fang *et al.* 2020; Das *et al.* 2021) within the area covered in the present study.

3. Results and discussion

3.1 H α emission-line stars

Slitless grism spectroscopy enables us to directly examine the point-like H α features of stars over the diffuse background emission (Herbig & Dahm 2001). We identified H α emission-line stars by analyzing slitless

spectroscopic images of the 11 overlapping sub-regions, each of $\sim 10 \times 10$ arcmin² area. Those stars with enhanced H α emission above the background are classified as emission-line stars. H α emission-line appears as a bright blob superposed over the continuum spectrum seen as a bright vertical line (see Figure 1, right panel). Therefore, sources showing bright spot along the slitless spectra are designated as H α emission stars. In total, we identified 131 emission-line stars in the present work. The spatial distribution of these stars is shown with the red circles in Figure 1. A list of these stars is given in Table 1.

3.2 Kinematics of identified H α stars

We searched for the Gaia EDR3 counterparts of the H α emission-line sources within a match radius of ~ 2 arcsec and obtained Gaia measurements for ~ 110 emission-line sources. We used the proper motion in RA (μ_α^*) and proper motion in declination (μ_δ) for the young stars to generate the vector point diagram (VPD), where $\mu_\alpha^* \equiv \mu_\alpha \cos(\delta)$. We restricted only those sources with proper motion uncertainty < 0.5 mas yr⁻¹ and G-band magnitude uncertainty < 0.1 mag. The VPD for those sources is shown in Figure 2. The over-density of sources can be easily noticed in Figure 2. The proper motion of the identified H α emission stars in the region peaks at $\mu_\alpha^*, \mu_\delta \sim -0.95(\pm 0.28), -3.57(\pm 0.58)$ mas yr⁻¹, which is comparable to the value found by Kuhn *et al.* (2020) for the stellar group ‘C’, in their work, which is at the same location as that of the area, we considered in this study. An area of radius about $3\text{-}\sigma$ (about 2.3 mas yr⁻¹) around the mean proper motion values of the H α emission-line stars is used to select the probable members (shown with green ellipse in Figure 2, left panel), and the remaining sources in the VPD are considered as field stars. There were only six emission-line stars, which seem to be non-members based on the VPD.

We also estimated the distance to the region using the parallax information of the H α emission stars having reliable parallax values ($\varpi/\sigma_\varpi > 5$) and are selected as proper motion members. These sources are shown with the red star symbols in Figure 2 (right panel). Except few outliers, the emission-line stars seem to have mean parallax values around 1.2 mas. After rejecting the outliers (i.e., sources with parallax values outside $\pm 3\sigma$ of the mean), the mean parallax value estimated for these sources is $\sim 1.223 \pm 0.077$ mas. We estimated the distance after correcting the mean parallax value for the known parallax offset of ~ -0.015 (Stassun & Torres 2021). The distance estimate for the region using

Table 1. A list of identified H α emission-line stars.

Sl. No.	RA (J2000.0) (°)	DEC (J2000.0) (°)	Flag
1	312.86059	+44.60798	919
2	312.91653	+44.55398	191
3	313.02814	+44.56527	101
4	312.92545	+44.64909	911
5	313.19233	+44.41601	199
6	313.09546	+44.53210	019
7	313.05975	+44.48682	119
8	313.06438	+44.46964	911
9	313.11137	+44.44232	991
10	313.07622	+44.41742	100
11	313.08189	+44.41378	111
12	313.06317	+44.38587	019
13	313.00413	+44.47816	111
14	312.99671	+44.42889	911
15	312.99410	+44.50163	009
16	312.88912	+44.44361	911
17	312.83750	+44.43878	911
18	312.84412	+44.42104	119
19	312.88662	+44.39667	111
20	312.83271	+44.38514	199
21	312.81887	+44.38278	110
22	313.02521	+44.28781	911
23	312.99760	+44.27282	911
24	312.99435	+44.24912	111
25	313.00074	+44.33306	111
26	312.96776	+44.30594	111
27	312.92462	+44.26895	111
28	312.92256	+44.25198	111
29	312.84837	+44.26183	111
30	312.86245	+44.22097	111
31	312.85172	+44.21787	111
32	312.82601	+44.21896	111
33	312.81672	+44.25008	111
34	312.86900	+44.26263	111
35	312.85063	+44.29911	119
36	312.85295	+44.30521	911
37	312.82535	+44.30353	911
38	312.83107	+44.32517	119
39	312.84446	+44.35214	111
40	312.95230	+44.08879	111
41	312.86117	+44.07353	911
42	312.85928	+44.08997	991
43	312.81256	+44.15019	011
44	312.89065	+44.17087	911
45	312.95324	+44.18422	111
46	312.92882	+44.12519	109
47	312.85861	+44.09017	999
48	312.86145	+44.07399	199
49	312.86820	+44.07723	900
50	312.88286	+44.04933	999
51	312.91099	+44.06148	911

Table 1. Continued.

Sl. No.	RA (J2000.0) (°)	DEC (J2000.0) (°)	Flag
52	312.95208	+44.08898	999
53	312.99204	+44.07230	191
54	313.05392	+44.34819	191
55	313.04382	+44.36894	019
56	313.05292	+44.32408	009
57	313.06306	+44.28903	019
58	313.07673	+44.27514	119
59	313.05867	+44.26504	911
60	313.09372	+44.23352	111
61	313.10560	+44.24240	199
62	313.11174	+44.28550	091
63	313.14334	+44.29481	111
64	313.13436	+44.31419	900
65	313.12020	+44.30853	111
66	313.14789	+44.31988	111
67	313.12866	+44.33646	910
68	313.13993	+44.34614	991
69	313.11794	+44.35423	111
70	313.12417	+44.35142	111
71	313.20216	+44.32875	900
72	313.17748	+44.32255	111
73	313.17749	+44.32255	119
74	313.25755	+44.31863	111
75	313.25351	+44.27050	111
76	313.24501	+44.25110	119
77	313.22359	+44.24906	199
78	313.21874	+44.24034	111
79	313.20781	+44.31744	111
80	312.81508	+44.24867	911
81	312.81065	+44.22721	111
82	312.81308	+44.30490	111
83	312.71904	+44.27894	111
84	312.74460	+44.29190	911
85	312.73183	+44.29729	191
86	312.72623	+44.29796	911
87	312.75654	+44.26169	110
88	312.69575	+44.29146	911
89	312.68728	+44.26535	919
90	312.63780	+44.26076	111
91	312.65429	+44.30686	111
92	312.80039	+44.31325	111
93	313.28738	+44.50291	111
94	313.30214	+44.51869	911
95	313.37614	+44.48684	111
96	313.38358	+44.48502	111
97	313.39493	+44.48834	911
98	313.39742	+44.46370	111
99	313.44332	+44.45117	111
100	313.37647	+44.44547	111
101	313.37959	+44.39075	111
102	313.37371	+44.39910	111

Table 1. Continued.

Sl. No.	RA (J2000.0) (°)	DEC (J2000.0) (°)	Flag
103	312.63470	+44.43819	111
104	312.61548	+44.39139	111
105	312.76938	+44.39725	111
106	312.76390	+44.40431	111
107	312.74483	+44.38817	110
108	312.72875	+44.38286	101
109	312.72158	+44.39822	911
110	312.76292	+44.40078	191
111	312.72327	+44.35025	919
112	312.70292	+44.34814	111
113	312.67791	+44.36552	911
114	312.65340	+44.36214	999
115	312.65577	+44.34832	111
116	312.65389	+44.34765	911
117	312.74766	+44.32776	111
118	312.74719	+44.33080	911
119	312.70334	+44.32317	911
120	312.78342	+44.53075	199
121	312.75411	+44.53063	119
122	312.78947	+44.55832	911
123	312.66787	+44.51364	111
124	312.66310	+44.51061	100
125	313.15198	+44.19623	111
126	313.04592	+44.13617	111
127	313.07698	+44.08767	111
128	313.11303	+44.07760	911
129	313.11698	+44.05859	911
130	312.72374	+44.35514	911
131	312.72488	+44.35520	911

Gaia data of emission line sources comes out to be $\sim 833 \pm 52$ pc, which is in agreement with that reported in previous works (e.g., [Bhardwaj et al. 2019](#); [Fang et al. 2020](#); [Kuhn et al. 2020](#)).

3.3 Color–magnitude diagrams: Evolutionary stages of $H\alpha$ stars

The evolutionary stages and physical parameters of the young stars can be well constrained using the optical observations ([Jose et al. 2017](#); [Panwar et al. 2017](#)). Locations of these stars on the optical color–magnitude diagrams (CMDs) can be utilized to confirm their evolutionary stages and formation mechanisms. We use optical photometry from Gaia EDR3 and PS1 surveys for the CMD analysis of the emission-line stars identified in the present work. Figure 3 illustrate the optical $G/G_{BP} - G_{RP}$ (left panel) and $g_{PS1}/(g_{PS1} - i_{PS1})$ (right panel) CMDs for all the stars (black dots) in the IC 5070 region.

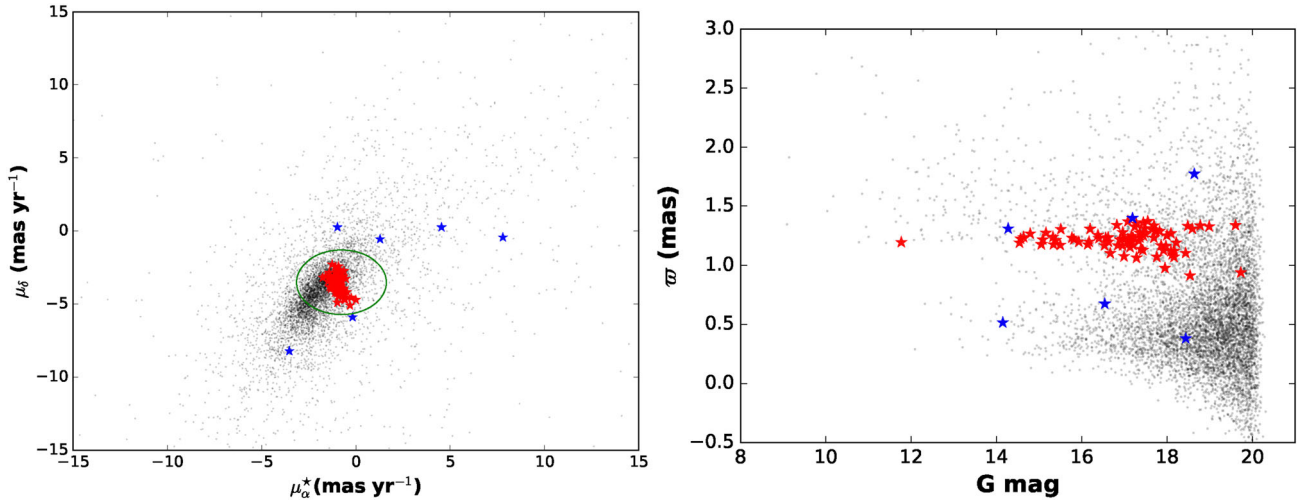


Figure 2. Vector point diagram (left panel) and parallax vs. magnitude (right panel) for the stars in the IC 5070 region. Black dots represent the sources within the region in Figure 1 and red star symbols are the $H\alpha$ emission line sources detected in the present survey. The green ellipse show the three- σ boundary around the mean proper motion values (see text).

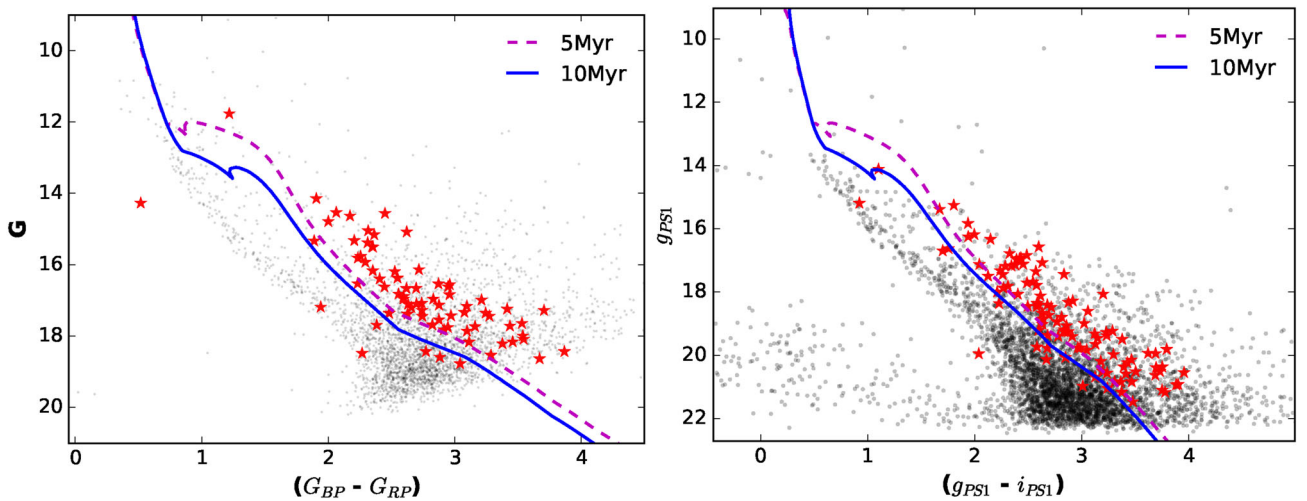


Figure 3. $(G_{BP} - G_{RP})/G$ Gaia (left panel) and $(g_{PS1} - i_{PS1})/g_{PS1}$ PS1 (right panel) CMDs for the stars in the IC 5070 region. Black dots represent all the sources within the region in Figure 1 and red stars are the $H\alpha$ emission line sources detected in the present emission-line stars survey. The dashed and continuous curves are the isochrones from PARSEC models for the ages 5 and 10 Myr, respectively, which are corrected for the adopted distance and average reddening of the region.

Star symbols represent the optical counterparts of emission-line stars in the region. Dashed and continuous curves are 5 Myr and 10 Myr isochrones for the solar metallicity taken from PARSEC (Pastorelli *et al.* 2020). The isochrones are shifted for the adopted distance (833 pc) and visual extinction $A_V \sim 2$ mag by adopting the extinction ratios mentioned in Wang & Chen (2019). In Figure 3, about 90% of the emission-line stars appear younger (< 5 Myr) and a few sources are of ages ~ 5 –10 Myr low-mass stars ($< 1.5 M_{\odot}$). The recent analysis by Pfalzner *et al.* (2022), shows that the median disk lifetime of

low-mass stars is generally in the range of ~ 5 –10 Myr, which is in agreement with the age distribution of $H\alpha$ emission line sources within IC 5070. In Figure 3, there are a few stars having ages > 10 Myr. These could be either non-members of the region or the stars formed prior to the formation of ionizing source of the region, with long-lived accretion disks, such as in Peter Pan disks (Silverberg *et al.* 2020). Detailed spectroscopic analysis is essential to understand the nature of these sources. The Gaia and PS1 CMDs for the emission-line sources detected in the present work, show that most of these are young members of the region with masses

$<1.5 M_{\odot}$, i.e., TTSs. We flagged about 14 emission-line sources with age >10 Myr as non-members.

Based on the astrometric and photometric data from Gaia and PS1, we have assigned flag to the $H\alpha$ emission-line stars cataloged in Table 1. The first digit in the column ‘Flag’ represents the membership status of the star based on the kinematics (PMs and/or parallax), the second digit shows the membership status based on the Gaia CMD and the third digit based on the PS1 CMD. Further, ‘1’ represents membership status ‘yes’, ‘0’ represents ‘no’ and ‘9’ represents ‘not confirmed’. Applying above criteria, we found that there are about 20 $H\alpha$ emission-line stars that are classified as non-members based on the PM/Parallax or Gaia CMD or PS1 CMD.

3.4 Nature of $H\alpha$ stars based on NIR color–color diagram

Young stellar sources exhibit excess emission in NIR wavelengths. Therefore, these sources can be identified and characterized based on their location in NIR color–color (CC) space. In Figure 4, we show the NIR $(J - H)/(H - K)$ CC diagrams for the $H\alpha$ stars. To construct the CC diagram, we have used the J , H , K measurements of the YSOs from Das et al. (2021), that were obtained from UKIDSS data archive. To avoid the chances of inclusion of saturated stars, we also used the 2MASS measurements for the stars, which were brighter than 13.25 mag in J -band. The thick red curve in the CC diagram represents the main-sequence (MS) locus, and the thick blue curve is the locus of the giants (Bessell & Brett 1988). The thin green line shows the classical TTS (CTTS) locus from Meyer et al. (1997). The three parallel black dashed lines drawn from the base of MS locus, the turning point of the MS locus and the tip of CTTS locus are the reddening vectors. All the magnitudes, colors and loci of the MS, giants and CTTS are converted to the Caltech Institute of Technology system and the extinction laws of Cohen et al. (1981) are adopted, i.e., $A_J/A_V = 0.265$, $A_H/A_V = 0.155$ and $A_K/A_V = 0.090$. The sources in the NIR CC diagram are classified into ‘F’, ‘T’ and ‘P’ regions (see Ojha et al. 2004) that are generally considered as ‘MS/evolved field stars or class III YSO candidates (weak-line TTSS)’, ‘class II YSO candidates (CTTSs)’ and ‘class I YSO candidates with circumstellar envelopes’, respectively. However, we note that the sources in the ‘T’ region may be reddened early-type MS stars with excess emission in the K-band (Mallick et al. 2013) and there may be an overlap of Herbig

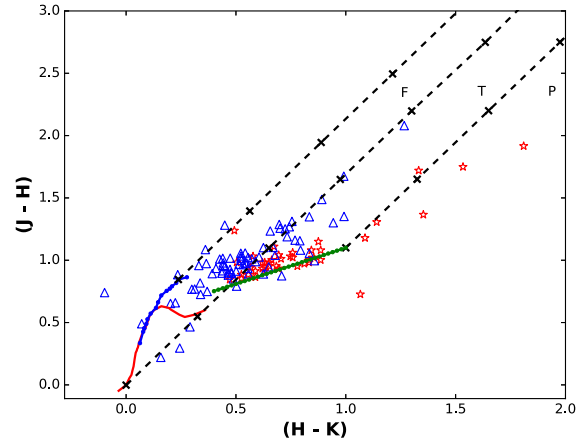


Figure 4. NIR color–color diagram for the emission-line stars in the IC 5070 region shown in Figure 1. NIR counterparts of $H\alpha$ emission stars taken from YSO catalog of Das et al. (2021) and 2MASS data are shown with star symbols and triangles, respectively. The thick red and blue curves represent the locus of the main-sequence (MS) stars and the giants, respectively (Bessell & Brett 1988). The thin green line shows the CTTS locus (Meyer et al. 1997). The three parallel black dashed lines drawn from the base of the MS locus, the turning point of the MS locus and the tip of the CTTS locus are the reddening vectors.

Ae/Be stars with the sources in the ‘T’ and ‘P’ regions, which generally occupy the place below the CTTS locus in the NIR CC diagram (for more details, see Hernández et al. 2005).

The NIR CC diagram of the $H\alpha$ stars clearly demonstrate that 100 $H\alpha$ emission line sources in our list are of classes II and III nature, implying that about 50% of the sources show IR excess on the NIR color–color diagram. We also estimated the visual extinction (A_V) towards the region by tracing the emission-line stars to the intrinsic locus for the TTSs. The average extinction for the emission-line stars in the region is ~ 2 mag.

3.5 Comparison with previous YSO catalogs

Das et al. (2021) identified YSOs in the whole NAP complex based on the NIR and mid-IR excess using UKIDSS and Spitzer-IRAC/MIPS data and found many clusterings of young stars including near IC 5070. They have also classified these young stars as class I, class II, class III and flat spectrum sources based on their NIR excess properties. To examine the evolutionary stages of emission-line stars, we also compared our emission-line star catalog with the YSOs catalog of Das et al. (2021) and found counterparts of 107 stars. Out of these 107 YSO candidates, one source is classified as class I, 88 as class II, 3 as class III, 14 as flat spectrum sources and one

is an unclassified source. Hence, most of the emission-line sources identified in the present work belongs to either class II or in transition from class I to class II stage (flat spectrum), indicating that $H\alpha$ emission line surveys are more efficient to detect thick disk bearing sources, i.e., actively accreting CTTS.

To know the spectral type of these emission-line sources, we also cross-matched our catalog to the recent spectroscopically confirmed member and non-member catalogs of Fang *et al.* (2020). We obtained spectral information corresponding to 96 emission line sources in our list. Most of these emission-line sources are of spectral types from K to M5. One of the emission-line star (#43) is classified as a non-member (see Fang *et al.* 2020), that has the parallax (0.52 mas) and hence, does not match with the mean parallax value of the young stars in the region. Hence, this is most probably a field star.

3.6 Star-formation history

Expanding HII region drives an ionization/shock fronts into the neighboring cloud, which may induce the formation of new stars due to the compression of pre-existing cores/clumps present inside the cloud in a process known as radiation driven implosion (RDI; Bertoldi 1989). As the outer part of the molecular cloud is getting ionized by the ionization front, the ionized gas from the molecular cloud flows (photo-evaporative flow) towards the ionizing source. This results the acceleration of cloud in the opposite direction, termed as ‘rocket effect’ (Oort 1954). As the remnant cloud slowly moves away from the ionizing star, an aligned distribution of the young stars formed due to the RDI, can be observed between the ionizing star and remnant cloud (Chauhan *et al.* 2009).

Small remnant molecular clouds, such as BRCs, globules and elephant trunks, are found to be associated with the recent star-formation activity and, in particular, BRCs are considered as ideal RDI candidates. The Pelican region consists of a bright-rimmed cloud (BRC 31) facing toward the ionizing star and contains many young stars near the bright-rim. Based on the distribution of ionized gas, bright rim, molecular gas and young stars; it is considered as one of the BRCs involved in the triggered star formation (Morgan *et al.* 2009).

In Figure 1 (left panel), we notice that $H\alpha$ emitters (mostly young stars) show an aligned distribution with respect to the ionizing star. As the kinematic information of most of the $H\alpha$ emission stars in the region is available, we examined the motion of these star

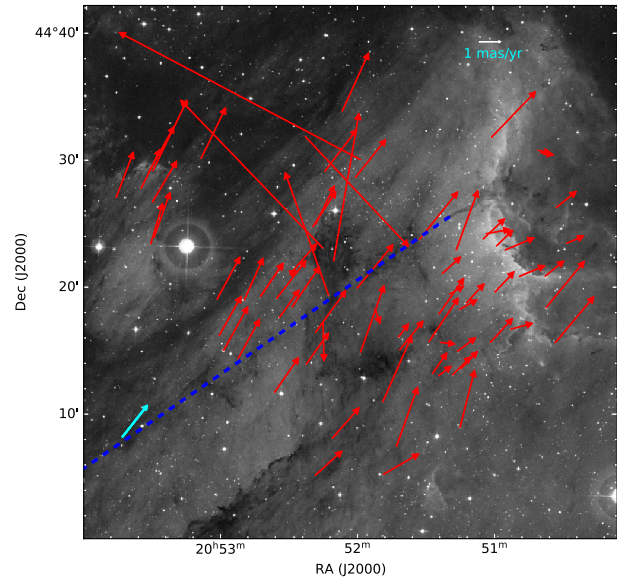


Figure 5. Proper motions of the emission line stars. The red arrows represent the relative proper motion vectors of the $H\alpha$ stars with respect to the ionizing star, obtained from Gaia EDR3. Blue dashed line indicates the directions of the main ionizing star. The cyan vector represents the mean proper motion of the $H\alpha$ stars with respect to the ionizing star.

with respect to the main ionizing source of the region, 2MASS J20555125+4352246. In Figure 5, vectors in red color show the direction of the proper motions of the emission line stars relative to the motion of the ionizing star. The direction of the ionizing source is shown with the blue dotted line. The cyan vector shows the mean proper motion of the emission-line stars relative to the proper motion of the ionizing star. The direction of the relative proper motion of emission-line stars is away from the ionizing source and seems almost parallel with the line joining the ionizing source to BRC 31. Our results are similar to that found by Saha *et al.* (2022a, b). Recently, Saha *et al.* (2022a) investigated the BRC 18 region based on the Gaia EDR3 proper motion information and suggested possibility of rocket effect scenario. However, we note that here, we have considered only the proper motions of the stars, and because we lack the radial velocity information of these stars, the above analysis represents only the projected motions of the stars on the sky plane.

4. Summary

In the present work, we report the results of our survey of emission-line stars in the star-forming region IC 5070 based on the slitless spectroscopic observations taken

with the 2m-HCT. The main findings of the present work are:

- We identified 131 H α emission-line sources in an area of ~ 0.29 degree² in the IC 5070 region.
- The Gaia EDR3 kinematic information of the identified emission-line stars suggest that a majority of sources share a similar proper motion, except few outliers. We calculated a mean proper motion values of $\mu_{\alpha}^* \sim -0.95(\pm 0.28)$, $\mu_{\delta} \sim -3.57(\pm 0.58)$ mas yr⁻¹, which are comparable to the previous works. We also used the Gaia EDR3 parallax measurements for these stars to estimate the distance of the region. Our estimated distance value of ~ 833 pc is similar to that found by Bhardwaj *et al.* (2019), Fang *et al.* (2020) and Kuhn *et al.* (2020).
- Using NIR CC diagram for these emission-line stars, we estimated the visual extinction $A_V \sim 2$ mag towards the region. Based on the CMDs constructed using Gaia and PS1 data, we found that most of the identified emission-line stars are young low-mass (mass $< 1.5 M_{\odot}$, age < 10 Myr), which is in agreement with the expected disk lifetime of low-mass mass stars.
- Based on the kinematics and photometry, we flagged the H α emission-line stars as members, non-members and non-confirmed sources.
- The relative proper motions of the emission stars with respect to the ionizing source suggests the possibility of the ‘rocket effect’ in BRC 31.

Acknowledgements

We are thankful to anonymous referee for providing the constructive comments, which have improved the manuscript. We thank the HTAC for time allocation and staff at the CREST and HCT for the support during observations. NP and RC acknowledge the financial support received through the SERB CRG2021/005876 grant and JJ acknowledges the financial support received through the DST-SERB grant SPG/2021/003850. This work has made use of data from the European Space Agency mission Gaia (<https://www.cosmos.esa.int/gaia>), processed by the Gaia Data Processing and Analysis Consortium (DPAC). Funding for the DPAC has been provided by national institutions, in particular, the institutions participating in the Gaia Multilateral Agreement. This publication also makes use of data from the Two Micron All Sky Survey, which is a joint project of the University of Massachusetts and

the Infrared Processing and Analysis Center/California Institute of Technology, funded by the National Aeronautics and Space Administration and the National Science Foundation. The Digitized Sky Surveys were produced at the Space Telescope Science Institute under U.S. Government grant NAG W-2166. The images of these surveys are based on photographic data obtained using the Oschin Schmidt Telescope on Palomar Mountain and the UK Schmidt Telescope. The Pan-STARRS1 Surveys were made possible through contributions by the Institute for Astronomy, the University of Hawaii, the Pan-STARRS Project Office, the Max-Planck Society and its participating institutes, the Max Planck Institute for Astronomy, Heidelberg, and the Max Planck Institute for Extraterrestrial Physics, Garching, The Johns Hopkins University, Durham University, the University of Edinburgh, the Queen’s University Belfast, the Harvard-Smithsonian Center for Astrophysics, the Las Cumbres Observatory Global Telescope Network Incorporated, the National Central University of Taiwan, the Space Telescope Science Institute and the National Aeronautics and Space Administration under grant no. NNX08AR22G issued through the Planetary Science Division of the NASA Science Mission Directorate, the National Science Foundation grant no. AST-1238877, the University of Maryland, Eotvos Lorand University (ELTE) and the Los Alamos National Laboratory.

References

- Bally J., Ginsburg A., Probst R., *et al.* 2014, AJ, 148, 120
 Bally J., Reipurth B. 2003, AJ, 126, 893
 Bertoldi F. 1989, ApJ, 346, 735
 Bessell M. S., Brett J. M. 1988, PASP, 100, 1134
 Bhardwaj A., Panwar N., Herczeg G. J., Chen W. P., Singh H. P. 2019, A&A, 627, A135
 Chambers K. C., Magnier E. A., Metcalfe N., *et al.* 2016, 1612.05560
 Chauhan N., Pandey A. K., Ogura K., *et al.* 2009, MNRAS, 396, 964
 Cohen J. G., Persson S. E., Elias J. H., Frogel J. A. 1981, ApJ, 249, 481
 Comerón F., Pasquali A. 2005, A&A, 430, 541
 Damiani F., Pillitteri I., Prisinzano L. 2017, A&A, 602, A115
 Das S. R., Jose J., Samal M. R., Zhang S., Panwar N. 2021, MNRAS, 500, 3123
 Fang M., Hillenbrand L. A., Kim J. S., *et al.* 2020, ApJ, 904, 146
 Findeisen K., Hillenbrand L., Ofek E., *et al.* 2013, ApJ, 768, 93
 Froebrich D., Scholz A., Campbell-White J., *et al.* 2018, RNAAS, 2, 61

- Gaia Collaboration 2020, VizieR Online Data Catalog, I/350
- Getman K. V., Kuhn M. A., Feigelson E. D., *et al.* 2018, *MNRAS*, 477, 298
- Ghosh A., Sharma S., Ninan J. P., *et al.* 2022, *ApJ*, 926, 68
- Gouliermis D. A. 2018, *PASP*, 130, 072001
- Guieu S., Rebull L. M., Stauffer J. R., *et al.* 2009, *ApJ*, 697, 787
- Gupta S., Jose J., More S., *et al.* 2021, *MNRAS*, 508, 3388
- Haro G. 1953, *ApJ*, 117, 73
- Hartmann L., Herczeg G., Calvet N. 2016, *ARA&A*, 54, 135
- Herbig G. H. 1954, *ApJ*, 119, 483
- Herbig G. H. 1958, *ApJ*, 128, 259
- Herbig G. H. 1998, *ApJ*, 497, 736
- Herbig G. H., Dahm S. E. 2001, *PASP*, 113, 195
- Herbig G. H., Dahm S. E. 2006, *AJ*, 131, 1530
- Herczeg G. J., Kuhn M. A., Zhou X., *et al.* 2019, *ApJ*, 878, 111
- Hernández J., Calvet N., Hartmann L., *et al.* 2005, *AJ*, 129, 856
- Ibryamov S., Semkov E., Milanov T., Peneva S. 2018, *RNAAS*, 18, 137
- Jose J., Herczeg G. J., Samal M. R., Fang Q., Panwar N. 2017, *ApJ*, 836, 98
- Jose J., Pandey A. K., Samal M. R., *et al.* 2013, *MNRAS*, 432, 3445
- Kuhn M. A., Hillenbrand L. A., Carpenter J. M., Avelar Menendez A. R. 2020, *ApJ*, 899, 128
- Laugalys V., Straižys V., Vrba F. J., *et al.* 2007, *Baltic Astronomy*, 16, 349
- Maíz Apellániz J., Sota A., Arias J. I., *et al.* 2016, *ApJS*, 224, 4
- Mallick K. K., Kumar M. S. N., Ojha D. K., *et al.* 2013, *ApJ*, 779, 113
- Meyer M. R., Calvet N., Hillenbrand L. A. 1997, *AJ*, 114, 288
- Morgan L. K., Urquhart J. S., Thompson M. A. 2009, *MNRAS*, 400, 1726
- Ogura K., Sugitani K., Pickles A. 2002, *AJ*, 123, 2597
- Ojha D. K., Ghosh S. K., Kulkarni V. K., *et al.* 2004, *A&A*, 415, 1039
- Oort J. H. 1954, *Bulletin of the Astronomical Institutes of the Netherlands*, 12, 177
- Panwar N., Samal M. R., Pandey A. K., Singh H. P., Sharma S. 2019, *AJ*, 157, 112
- Panwar N., Samal M. R., Pandey A. K., *et al.* 2017, *MNRAS*, 468, 2684
- Pastorelli G., Marigo P., Girardi L., *et al.* 2020, *MNRAS*, 498, 3283
- Pettersson B., Reipurth B. 2019, *A&A*, 630, A90
- Pfalzner S., Dehghani S., Michel A. 2022, *ApJL*, 939, L10
- Poljančič B. I., Jurdana-Šepić R., Semkov E. H., *et al.* 2014, *A&A*, 568, A49
- Rebull L. M., Guieu S., Stauffer J. R., *et al.* 2011, *ApJS*, 193, 25
- Reipurth B., Schneider N. 2008, in ed Reipurth B., *Handbook of Star Forming Regions*, Vol. 4, p. 36
- Saha P., Gopinathan M., Ojha D. K., Neha S. 2022a, *MNRAS*, 510, 2644
- Saha P., Maheshwar G., Ojha D. K., Baug T., Neha S. 2022b, *MNRAS Letter*, 515, 67
- Silverberg S. M., Wisniewski J. P., Kuchner M. J., *et al.* 2020, *ApJ*, 890, 106
- Sota A., Maíz Apellániz J., Walborn N. R., *et al.* 2011, *ApJS*, 193, 24
- Stassun K. G., Torres G. 2021, *ApJL*, 907, L33
- Wang S., Chen X. 2019, *ApJ*, 877, 116
- Westerhout G. 1958, *Bulletin of the Astronomical Institutes of the Netherlands*, 14, 215
- Zucker C., Speagle J. S., Schlafly E. F., *et al.* 2020, *A&A*, 633, A51